Metrology systems of Hobby-Eberly Telescope wide field upgrade

Lee, Hanshin, Hill, Gary, Cornell, Mark, Vattiat, Brian, Perry, Dave, et al.

Hanshin Lee, Gary J. Hill, Mark E. Cornell, Brian L. Vattiat, Dave M. Perry, Tom H. Rafferty, Trey Taylor, Michael Hart, Marc D. Rafal, Richard D. Savage, "Metrology systems of Hobby-Eberly Telescope wide field upgrade," Proc. SPIE 8444, Ground-based and Airborne Telescopes IV, 84444S (27 September 2012); doi: 10.1117/12.926732

SPIE.

Event: SPIE Astronomical Telescopes + Instrumentation, 2012, Amsterdam, Netherlands

Metrology Systems of the Hobby-Eberly Telescope[1] Wide Field Upgrade

Hanshin Lee [a,2], Gary J. Hill[a], Mark E. Cornell[a], Brian Vattiat[a], Dave Perry[a], Tom Rafferty[a], Trey Taylor[a], Michael Hart[b], Marc D. Rafal[a], and Richard Savage[a]

[a] McDonald Observatory, University of Texas at Austin, 2515 Speedway Stop 1402, Austin, TX 78712-0259, USA
[b] Hart Scientific Consulting International L.L.C., 5434 E. Burns St., Tucson, AZ 85711, USA

ABSTRACT

The Hobby-Eberly Telescope (HET) Wide-Field Upgrade (WFU) will be equipped with new closed-loop metrology systems to actively control the optical alignment of the new four-mirror Wide-Field Corrector (WFC) as it tracks sidereal motion with respect to the fixed primary mirror. These systems include a tip/tilt camera (TTCam), distance measuring interferometers (DMI), guide probes (GP), and wavefront sensors (WFS). While the TTCam and DMIs are to monitor the mechanical alignment of the WFC, the WFSs and GPs will produce direct measurement of the optical alignment of the WFC with respect to the HET primary mirror. Together, these systems provide fully redundant alignment and pointing information for the telescope, thereby keeping the WFC in focus and suppressing alignment-driven field aberrations. In addition to these closed-loop metrology systems, we will have a pupil viewing camera (PVCam) and a calibration wavefront sensor (CWFS). The PVCam will be used for occasional reflectance measurement of the HET primary mirror segments in the standard R,G,B colors. The CWFS will provide the reference wavefront signal against which the other two WFS are calibrated. We describe the current snapshot of these systems and discuss lab/on-sky performance test results of the systems.

Keywords: Metrology Systems, Hobby-Eberly Telescope, HETDEX

1. INTRODUCTION

Over the next year or so, the Hobby-Eberly Telescope (HET) will be upgraded with a 22 arc-minutes diameter field of view wide field corrector (WFC), a new tracker and prime focus instrument package (PFIP), and new metrology systems to support the Hobby-Eberly Telescope Dark Energy experiment (HETDEX)[1][2]. The new corrector has improved image quality and a 10-meter pupil diameter[3]. The periphery of the field (i.e. an annular field from 16 arc-minutes to 22 arc-minutes diameter, called the metrology service field) will be used for guiding and wavefront sensing to provide the necessary feedback to keep the telescope correctly aligned. The WFC will give 30 times larger observing area than the current HET corrector. It is a four-mirror design with two concave 1-meter diameter mirrors, one concave 0.9-meter diameter mirror, and one convex 0.23-meter diameter mirror. The corrector is designed to feed optical fibers at f/3.65 to minimize focal ratio degradation, and so the chief ray from all field angles is normal to the focal surface. This is achieved with a concave spherical focal surface centered on the exit pupil. The imaging performance of the WFC alone is 0.5 arc-seconds or better over the entire 22 arc-minutes field of view, and vignetting is minimal. As in the current HET, the WFC will track sidereal motion with respect to the optical axis of the fixed spherical primary mirror (M1). Therefore, the WFC needs to be continuously positioned and oriented to maintain its alignment in order to deliver the required image quality. This demands closed-loop control of the positions of the WFC. Table 1 shows the allowed ranges of misalignments of the WFC as a rigid body at any given track position. Figure 1 shows the overview of the WFU metrology systems.

Table 1. The allowed ranges of misalignments of the WFC.

Alignment parameters	Decenter	Defocus	Tip/tilt	Rho
Requirement	±10μm	±10μm	±4arcsec.	±20arcsec.

The feedback to keep these alignment specifications requires robust metrology and we plan to deploy the following closed-loop metrology subsystems for this:

- Guide probes (GP): Monitoring the position on the sky, plus plate scale of the optical system, and monitor the image quality and atmospheric transparency plus field rotation correction.

[1] The Hobby-Eberly Telescope is operated by McDonald Observatory on behalf of the University of Texas at Austin, the Pennsylvania State University, Ludwig-Maximillians-Universität München, and Georg-August-Universität, Göttingen.
[2] Hanshin Lee: E-mail: lee@astro.as.utexas.edu

Ground-based and Airborne Telescopes IV, edited by Larry M. Stepp, Roberto Gilmozzi, Helen J. Hall,
Proc. of SPIE Vol. 8444, 84444S · © 2012 SPIE · CCC code: 0277-786/12/$18 · doi: 10.1117/12.926732

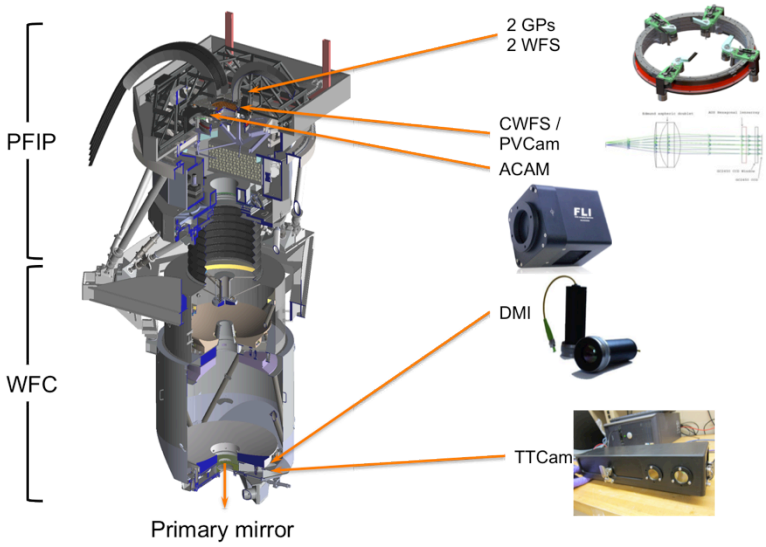

Figure 1 The overview of the WFU metrology systems.

- Wavefront sensors (WFS): Monitoring the plate-scale, focus, and tilt of the WFC.
- Distance measuring interferometer (DMI): Monitoring the physical distance between the WFC and primary mirror.
- Tip-Tilt Camera (TTCam): Monitoring the physical tip/tilt of the WFC with respect to the optical axis of the primary mirror.
- Acquisition Camera (ACAM): For initial field identification, telescope pointing.

The wavefront sensor is a newly introduced metrology system to the HET in order to close the loop on all axes of the system together with the DMI and TTCam adapted from the current tracker metrology system. Both operate at a near infrared wavelength[5]. These systems can provide sufficient redundancy for the highest possible reliability in monitoring the alignment of the WFC. The DMI and TTCam measurements are directly related to the alignment state of the mechanical structure of the WFC, while responses from the WFS and GP are analyzed to determine the "*optical*" alignment state of the WFC. The WFS analysis is based on the following alignment–aberration relations: Decenter of the WFC causes systematic wavefront tilts across the field. This is equivalent to the telescope pointing error and equivalent to the stellar position measurement from the GP. Tilt errors add field constant coma to the aberration field of the WFC, while the axial motion introduces defocus aberration that is also field constant. The defocus aberration, however, can also be produced when the global radius of curvature (GRoC) of M1 changes. As this variation can also produce plate scale variation, an appropriate monitoring system is necessary. Although the Segment Alignment Maintenance System (SAMS) maintains the positions of the 91 mirror segments with respect to each other [6], it is less sensitive to the GRoC change. Thus, we plan to monitor the GRoC variation by the combination of focus position from the WFS with the physical distance measurement from the DMI and to verify this by the plate scale measured from the positions of guide stars on the GP and WFS. The feedback from the SAMS can be used as a redundant piece of information on the GRoC change. The primary mirror tip/tilt is currently controlled by the Mirror Alignment Recovery System (MARS). MARS maintains the segment tip/tilt to an accuracy of 0.14 arc-seconds rms[7]. We plan to continue using this system for the WFU. We also plan to use three DMIs to correct the segment piston errors. For this, we will deploy three DMI heads connected to common sources to reach all mirror segments across M1. The DMI, TTCam, GP, and WFS systems can provide fully redundant closed-loop alignment and pointing information for the telescope, thereby keeping the WFC in focus and suppressing alignment-driven field aberrations.

In addition, there will be a pupil-viewing camera (PVCam) and a calibration wavefront sensor (CWFS). The PVCam will image the telescope pupil (therefore the M1 segments and the moving baffle at the exit pupil of the WFC) in the standard R,G,B colors. This will enable us to monitor the reflectance of the segment mirror coating. A time series of the mirror segment reflectance will be recorded from the point where the segments are coated. Occasional relative reflectance comparison will provide the level of coating degradation. It will also be used to monitor the moving baffle position. The CWFS will have denser sub-apertures than the WFS will have. This will enable finer sampling of the telescope wavefront error and thus can provide reference signals against which the WFS are calibrated. We presented the status of some of the metrology systems two years ago[4] and this paper presents the update of the progress made so far for those systems and additional systems that were not described back then.

2. WFU METROLOGY SYSTEMS

On the HET, the optical alignment of the WFC with respect to the M1 must be held dynamically while the image moves as much as 3.8 m with respect to the main telescope structure along the M1 focal sphere. The mechanisms controlling the tracker synthesize the required tracker motions along the focal sphere by a combination of X, Y, focus (W), tip (θ), tilt (φ), rotation (ρ) axes of stacked X and Y stages, a hexapod system and a rotation stage. The range of motion for each axis is: 3.8 m in x and y, 130 mm in z, 17° in θ and φ, and 44° deg in ρ (Figure 2). In the very original design of the

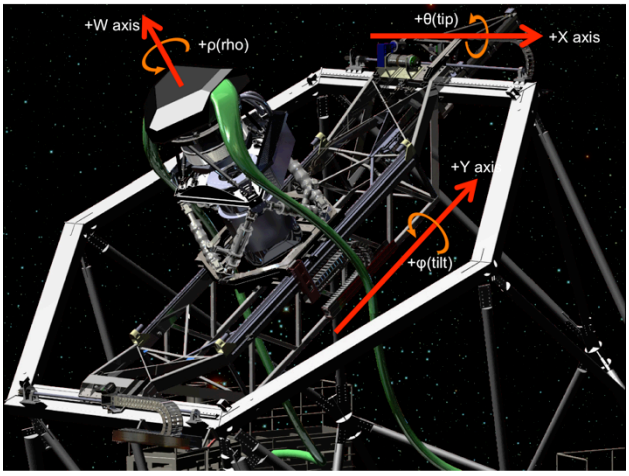

Figure 2 WFU Coordinate system.

telescope the only feedback to control the motion with respect to the M1 was provided by a guider, which constrained only the two pointing degrees of freedom. The remaining degrees of freedom were to be modeled. To overcome the deficiencies of the mount-models, additional metrology systems were added to provide feedback on focus, and tip and tilt of the corrector with respect to M1. Focus is measured with an absolute distance measuring interferometer (DMI) while tip and tilt are measured with an auto-collimator system called the tip/tilt camera (TTCam)[4]. Both the DMI and TTCam operate at a wavelength of 1.55 μm that is outside the range of any current or planned instrument used on the HET. These two systems are to be directly adopted for the same metrology in the WFU. In order to close the alignment control loop on all axes for the WFU, we plan to add wavefront sensors to the suite of metrology systems. In conjunction with the guide probes, the WFS will provide direct information on the *optical alignment state* of the WFC. For the purpose of calibrating the WFS, the CWFS will also be installed. For the M1 mirror segment reflectance monitor, the PVCam will be used. The individual metrology sub-systems are detailed below.

2.1 Distance Measuring Interferometer (DMI)

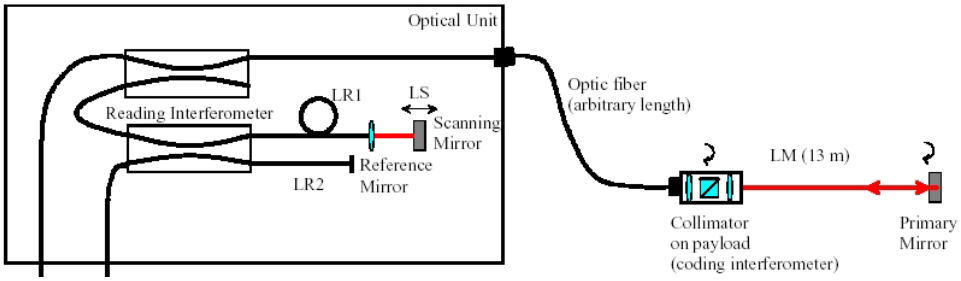

Figure 3 The operation principle of the distance measuring interferometer.

The DMI is a low-coherence distance measuring interferometer developed by Fogale-Nanotech[8]. The system operation is based on a pair of Michelson interferometers where all of the optical paths, except the measurement arm, are along optical fibers (Figure 3). The first interferometer encodes the phase difference to the primary mirror with respect to a reference at the collimator measurement head, a distance equal to 2LM. The two arms of the second interferometer induce phase delays of 2(LR1+LS) and LR2 respectively. Here, LS can be adjusted by an optically encoded scanning mirror. The second interferometer reads the phase difference from the coding interferometer by scanning through the exact phase matching condition where LR1+LS-LR2 = LM. The system light source is a polychromatic super-luminescent diode (SLED). An interference signal is detected only when the phase difference is less than the coherence length of the source and is modulated by a peaked function called the visibility curve. Figure 4 shows an example of an interference curve. The peak of the visibility curve occurs at the exact phase matching condition of LR1+LS-LR2 = LM. This configuration allows the compact measurement head (Figure 5) of the instrument to be mounted remotely. The length of the optical

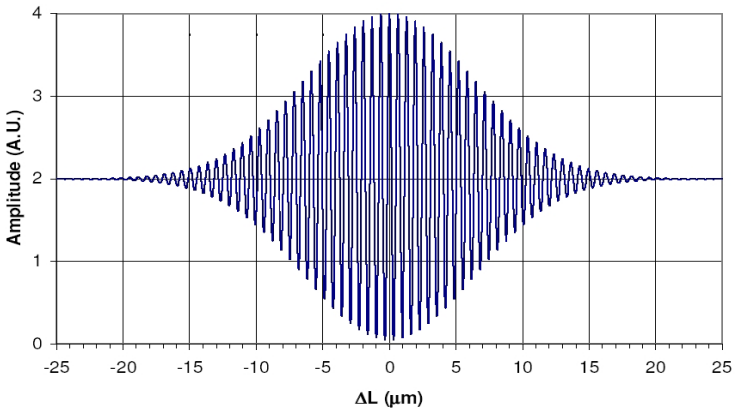

Figure 4 An example interference curve. The peak of the visibility curve occurs at the exact phase matching condition of LR1+LS-LR2 = LM. The absolute distance is obtained by finding the peak.

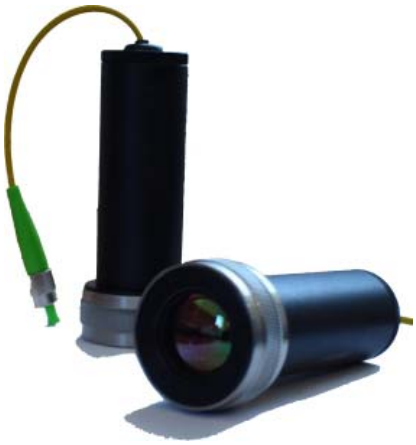

Figure 5 The DMI measurement heads with a focusing lens at the output end of the head.

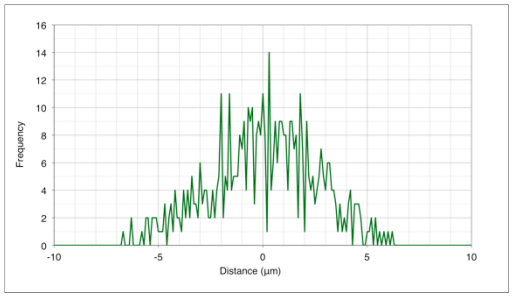

Figure 6 The repeatability measurement of the current HET DMI.

fiber feeding the measurement head can be arbitrary and the distance measurement is unaffected by thermally induced changes to the length of feed fiber. The reading interferometer is housed in a thermally controlled chamber to maintain stability. The absolute distance is obtained by finding the peak. The range of the scanning mirror is 40 mm. This allows a sufficiently wide range for locating and setup of the measurement head that can be scanned in 5 sec. The scanning range is in fact narrower than 40 mm to reduce the measurement time. The visibility curve is sampled in 10ms. The RMS repeatability of measurements is 2.5 μm over time scales several minutes (Figure 6). The long-term accuracy is specified at 1ppm[8].

The system currently installed at the HET has two channels: one is to measure a nominal distance of approximately 12.6 m, located at the current corrector, and used for tracker metrology, and the other channel is set to measure a nominal distance of approximately 26.2m to measure distances at the center of curvature of the primary mirror. For the WFU, we plan to add two more DMI heads, thus three DMI heads sharing one two-channel DMI source. The DMI heads are to be located within the WFC in such a way that we can measure physical distances between the WFC and all mirror segments and the piston map of the entire M1 mirror segments can be obtained, which is otherwise difficult with only one DMI on the WFC. Each head will have its optical axis passing through the center of curvature (CoC) of the M1. This approach is expected to make a better correction to the M1 mirror segment piston errors.

2.2 Tip Tilt Camera (TTCam)

The basic design concept of the new TTCam (as shown in Figure 7) is similar to the current one. The TTCam consists of a fiber-coupled light source and a collimator. The light source is an amplified spontaneous emission (ASE) source from Lightwaves2020.

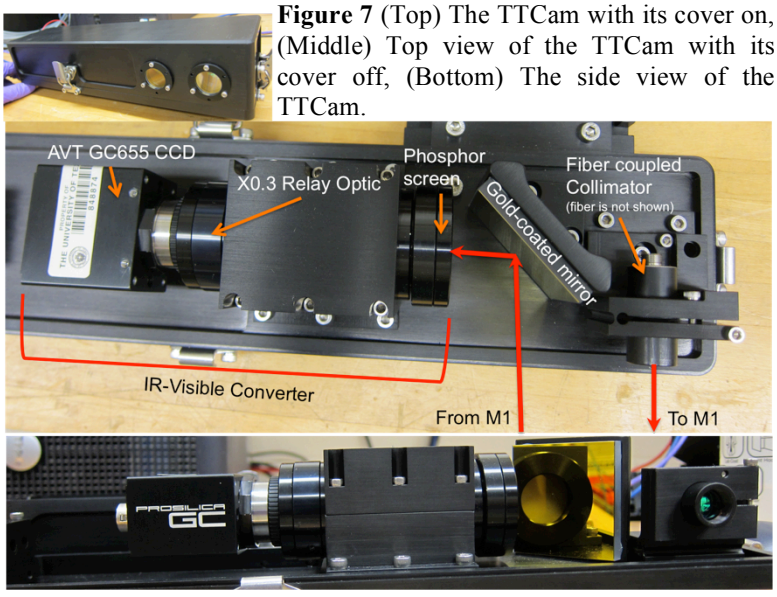

Figure 7 (Top) The TTCam with its cover on, (Middle) Top view of the TTCam with its cover off, (Bottom) The side view of the TTCam.

The source has the central wavelength at 1.55 μm with a spectral width of approximately 50 nm, which eliminates problems with fringing due to a laser source and forms a smooth Gaussian-like PSF. The collimated beam passes through a window and then focused by a mirror segment on reflection. The beam optical axis is slightly tilted so that the returned beam makes an angle with respect to the collimated beam. The return beam passes through another window. The beam is then folded by a gold-coated fold mirror to an IR converter with a camera attached (Edmund Optics). The converter has a phosphor screen where the returned beam is focused. The IR spot on the screen is then converted into a visible spot so that the camera can reimage it onto a machine vision CCD sensor (Allied Vision Technology (AVT) Prosilica GC655, 659×493 pixels, 9.9μm pixel, 12bit). The magnification is ×0.33 therefore the capture range of the TTCam is 160×120 sq. arc-seconds. The entire TTCam assembly will be mounted to the side of the M3 strong back of the WFC.

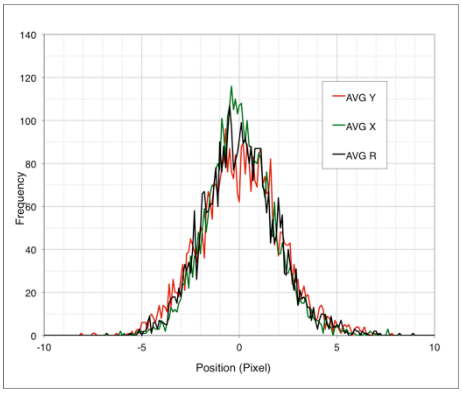

Figure 8 The repeatability measurement of the current HET TTCam. The pixel scale is 0.145 arc-seconds.

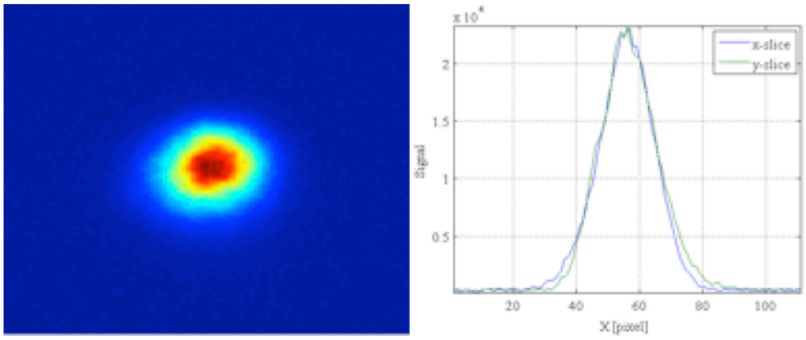

Figure 9 (Left) The spot imaged through the IR-Visble converter and (Right) Horizontal and vertical slices of the spot.

The TTCam installed in the current corrector was developed in house due to the lack of a commercial product operating in the near infra-red which met our specifications for accuracy, stability and capture range[5]. The current TTCam projects a collimated beam at a normal to the primary mirror and the return beam is focused by a mirror segment and steered by a beam-splitter to a camera with a phosphor coated CCD yielding a spot size of 2 mm. The current TTCam has a capture range of 150 arc-seconds and rms repeatability of 0.3 arc-seconds (Figure 8). In a previous prototype with the same IR-Visible converter and light source[4], we have measured the image centroid stability (Figure 9). The stability in the current test setup is less than a tenth of a pixel. The source power of 0.8 mW produces sufficiently high signal-to-noise ratio (SNR ~ 3800).

2.3 Guide Probe (GP) and Wavefront Sensor (WFS)

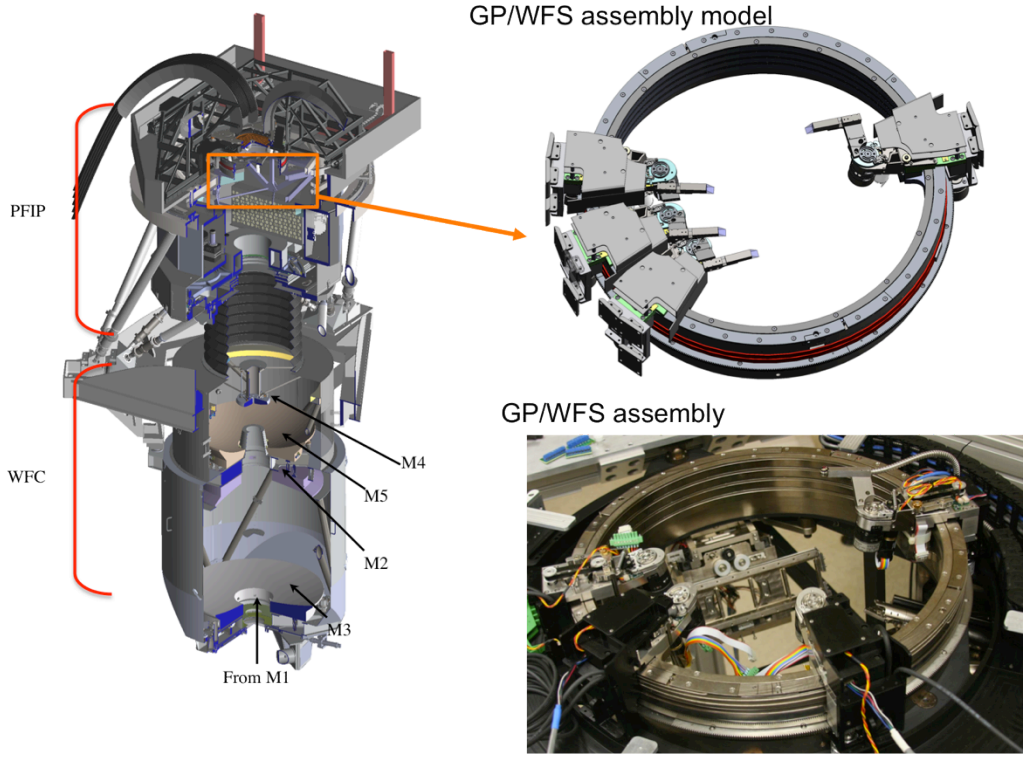

Figure 10 (Left) A section view of the WFC and PFIP where the guide probe and wavefront sensor assembly reside near the focal surface (marked by orange rectangle near the top of the PFIP). (Top right) A close-up view of the guide probe and wavefront sensor assembly where two guide probes and two wavefront sensor probes are mounted on a

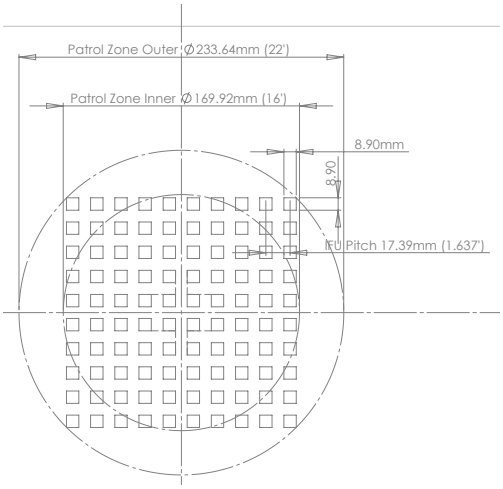

Figure 11 The layout of the WFU focal plane and the metrology service field.

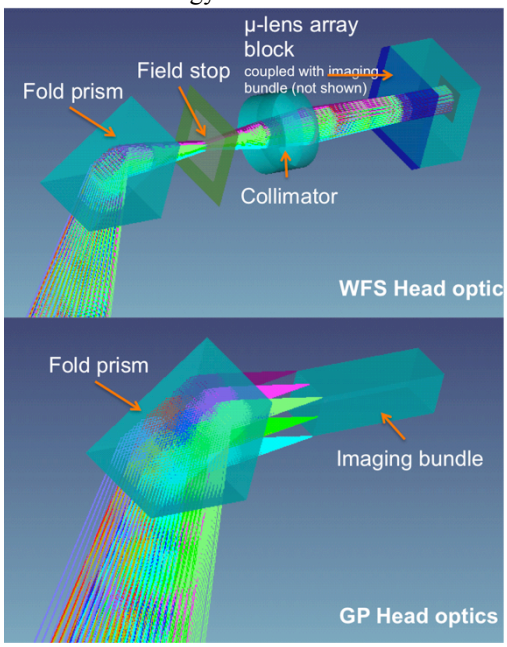

Figure 12 The WFS and GP head optics optical models.

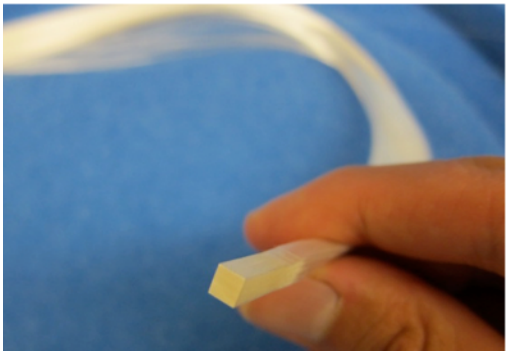

Figure 13 The imaging fiber bundle used in the GP/WFS assembly.

circular bearing; each probe has a probing arm; a folding prism is at the tip of each arm, steering the beam from the WFC to an imaging fiber bundle (guide probe) or to a collimation lens that feeds a collimated beam to a lenslet array butted to an imaging fiber bundle (wavefront sensor) (optical components are not shown). (Bottom right) The actual GP/WFS assembly under construction is shown.

Figure 10 illustrates the layout of the WFC and Prime-Focus Instrumentation Package (PFIP). The guide-probe (GP) and wavefront sensor (WFS) assembly resides near the focal surface assembly marked by an orange rectangle near the top of the PFIP. A close-up view of the GP/WFS assembly model is shown on the top right and the actual assembly under construction and test is shown at the bottom of Figure 10.

There are four probes; two are GP and two are WFS probes. Each GP and WFS probe patrols the metrology service field in the WFU focal plane (i.e. an annular field from 16′ to 22′ diameter, see Figure 11). Each probe has its own head optics in the GP/WFS assembly (Figure 12). A folding prism is placed at the tip of the head i) to route the beam within the metrology service field into a pupil imaging optics that forms Shack-Hartmann (SH) spots on an imaging fiber bundle for WFS or ii) to directly feed an imaging fiber bundle for GP. The imaging fiber bundles transmit stellar images (for GP) or a SH image (for WFS) to the output systems located in a remote electronic box of the PFIP. The field stop in the WFS head defines a field of view of 4.5 x 4.5 sq. arc-seconds. The GP field of view is defined by the size of the input matrix of the imaging bundle (4x4 sq. mm or 22.6x22.6 sq. arc-seconds on the sky) (Figure 13). At the time of this writing, we are procuring the imaging bundles from Schott.

Each imaging bundle feeds an output system that consists of a relay optic and a CCD sensor (Figure 14). In the GP, the beam speed at the input end of the imaging bundle is f/3.65. It has been measured that the beam speed at the output end of the imaging bundle is f/2 due to the focal ratio degradation (FRD) [9]. Therefore, the relay optics in the GP output system is designed to be able to accept f/2 beams. There are total 6 spherical lens elements (2 doublets and 2 singlets) in each GP relay system (Jenoptik fabricated the lenses). The relay system converts f/2 into f/3, thus x1.5 magnification. The GP output relay is equipped with a set of Johnson B, Sloan g, r, i, and clear filters so that the GP measurements can be used as additional flux calibration inputs for the HETDEX science data calibration. The CCD sensor is Finger Lakes Imaging (FLI) Microline MLx285 that uses a Sony ICX285AL monochromatic 16-bit CCD chip. The pixel format is 1434x1050 with 6.45μm pitch. The pixel scale of the GP is 0.024 arc-second per pixel, thus we plan to bin by 8 times at least. The recorded stellar images in the GP are analyzed to determine the centroids and thus the correction to the telescope pointing, to assess the image quality, and to monitor the telescope plate scale variation. The guide star image will also be used to determine atmospheric transparency and to generate flux calibration data for the HETDEX science data reduction. The expected guiding accuracy is 0.25 arc-seconds with 0.1 arc-seconds as a goal. One of the assembled WFS head is shown in Figure 15. It shows the folding prism at the tip of the probe followed by a field stop and collimation lens (not shown) in side the rectangular housing. The micro-lens array block is glued to

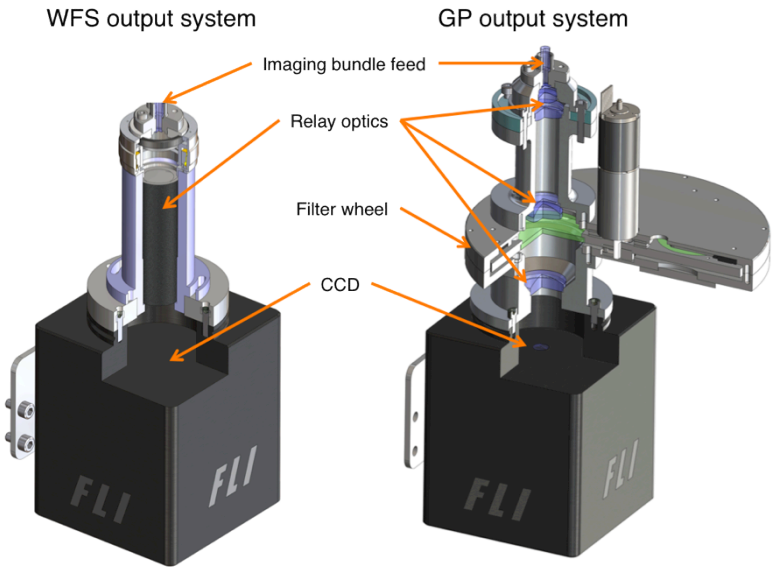

Figure 14 The WFS and GP output system section view.

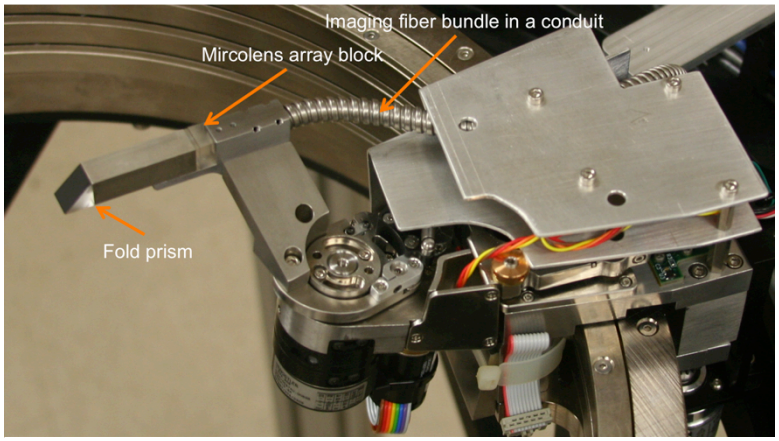

Figure 15 One of the assembled WFS probe head in the GP/WFS assembly.

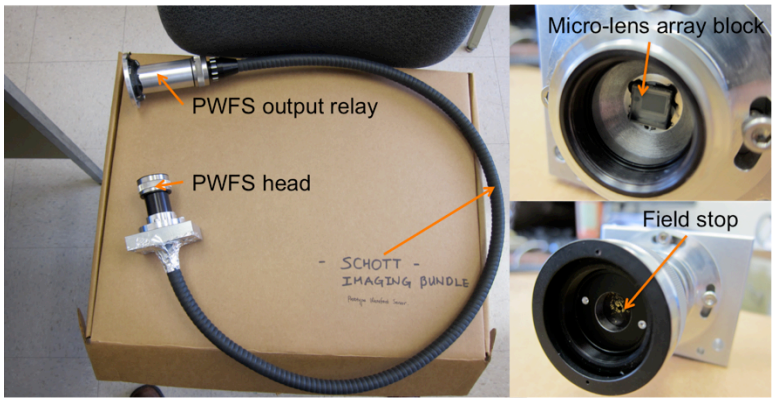

Figure 16 The solid model of the Prototype-WFS.

the end of the housing. The side surfaces of the micro-lens array block will be painted. The imaging fiber bundle (inside the metal conduit) is glued to the exit face of the micron-lens array block.

In the WFS, each sub-aperture feeds the imaging bundle at f/16. Our lab measurement indicated that, at this input speed, the output beam comes out at f/4.5 or slower due to FRD in the imaging bundle. We have identified an off-the-shelf 1:1 f/4 finite-conjugate relay system from Edmund Optics as a suitable output relay optic for the WFS. We have successfully used this relay in a prototype WFS (PWFS, see below for further descriptions). The WFS operates without filters and uses the same FLI Microline CCD. The sub-aperture grid is 11x11 and, at any given tracker position, at least 45 sub-apertures are in full or partial illumination. This allows us to determine the first 22 Zernike aberration coefficients (or up to radial order 6), among which the first 7 terms are explicitly used to determine the correction to the WFC alignment, in particular focus and tip/tilt. The WFS can reach SNR ~ 70 in a 60sec exposure for m_v=18 stars with 5e- rms read noise. This can lead to 0.07 arc-seconds SH spot centroid accuracy in rms at a worst case. The expected intrinsic WFC alignment estimation accuracy from the WFS is ±1.5 μm in decenter, ±2.5 μm in focus, ±0.7 arc-seconds in tip/tilt, and ±1.5 arc-seconds in rho in peak-to-valley[10]. Ideally, we wish to have stars for two guide probes and two wavefront sensors, each operating in one quadrant of the metrology service field, but the current baseline is to have at least two guide stars and one wavefront sensor star.

Since SH wavefront sensing has never been used at the HET and the concept of re-routing the SH image through a coherent imaging bundle is new, we built the PWFS in early 2011. Figure 16 shows the solid model of the PWFS. The PWFS head consists of a pinhole mask acting as a 6.7 arc-seconds diameter field stop, a collimator lens (focal length of 21.5mm from Edmund Optics) in a barrel, a micro-lens array block (square micro lenses with 300μm pitch on a fused silica substrate), and an imaging fiber bundle from Schott (IG-567, 6.7mm x 5mm input/output fiber matrix with 10μm fibers

and a standard C-mount). The current HET has a 9.25m-diameter pupil and beam speed is f/4.62. The re-imaged telescope pupil is 4.8mm in diameter, with 16 sub-apertures across the diameter. The micro-lens array samples the sub-apertures and produces a SH image onto the back face of the lens array block which is coupled with the input matrix of the imaging bundle by optical couplant. The SH image is then transferred through the imaging bundle to the output input matrix which feeds the output relay system. The relay is an off-the-shelf 1:1 f/4 imaging system from Edmund Optics and is identical to the relay to be used in the WFS of the GP/WFS assembly. The relay system re-images the output matrix onto a CCD (FLI Microline front-side illuminated ML0261E, 20μm pixel size, 512x512 format, dark current of 0.7e-/pixel/sec, 9e- rms read-out-noise, full-well depth of 200,000e-, peak QE of 0.58). The pixel scale on the CCD is 0.21 arc-seconds. We used a calibration pinhole (50μm in diameter) mounted in a focus-adjustable barrel with a set screw so that the distance to the collimator lens can be fine adjusted and then locked. In the output relay, we used the same focus adjustable barrel between the output end of the bundle and the relay optics. Using these adjustments and broadband light source, we calibrated the SH spot grid against the Zemax model of the whole system and the known fabrication tolerances of the individual optical/mechanical components.

In the lab, we fed the PWFS with a f/4 beam produced by another imaging system that was on a three-axis stage (x,y,z). We intentionally mis-aligned the system by known amounts and then estimated the misalignments from the PWFS signal. For 10 case experiments, we obtained the estimation accuracy of 1μm at 99% level in decenter (i.e. x and y) and focus (i.e. z) within the range of ±20μm. As the amount of mis-alignment increases, the estimation accuracy tended to asymptote at 5% to 10% of the input mis-alignment. When the estimated values are plotted against the input values, it appears as a linear line with a slope between 0.9 and 0.95.

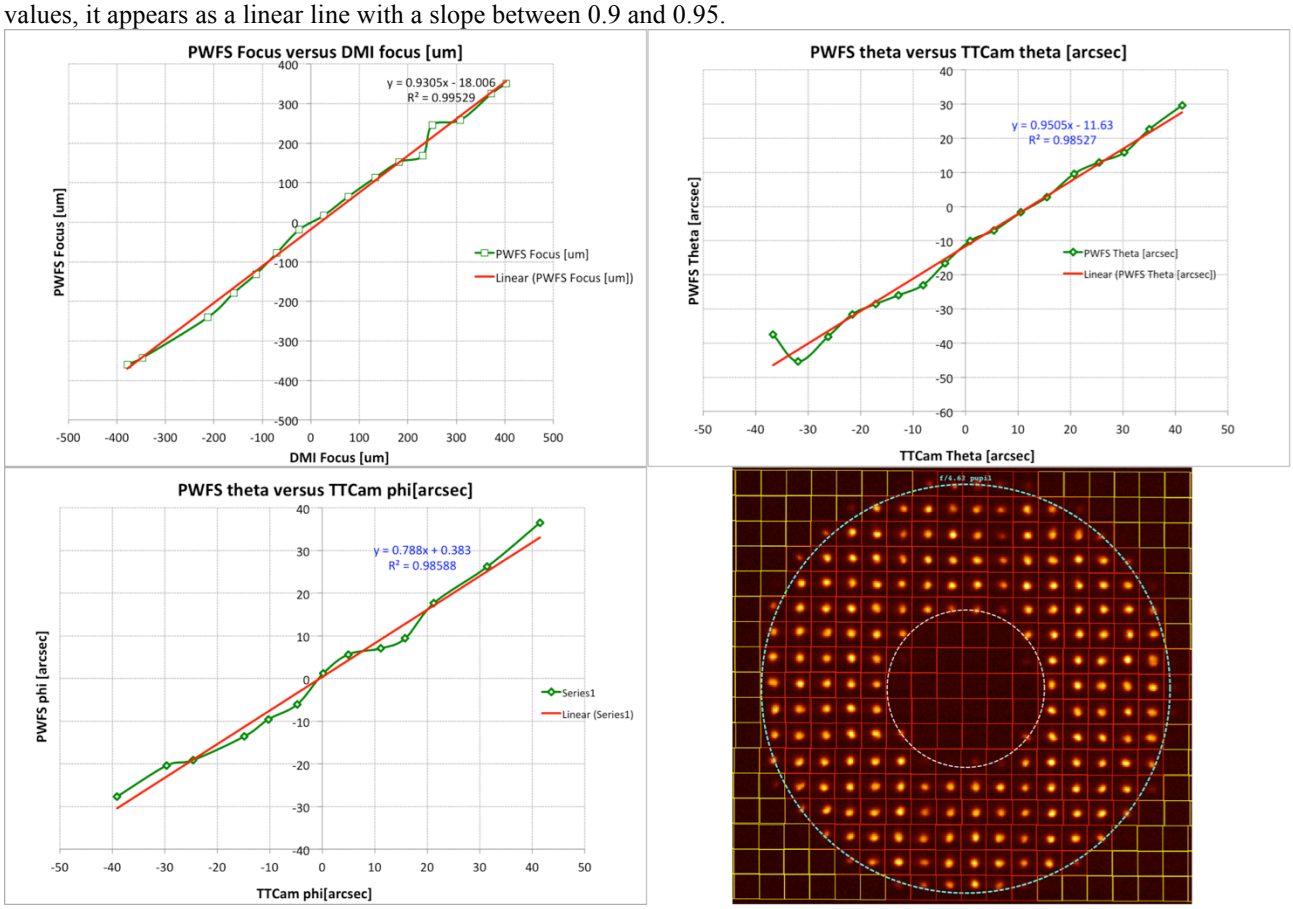

Figure 17 The result from the HET PWFS run in April 2011. The correlation between the PWFS estimate and the DMI/TTCam output in (Top-left) focus, (Top-right) tilt or theta, (Bottom-left) tip or phi. (Bottom-right) A sample SH image from the PWFS.

On April 5 2011, we conducted an on-sky test of the PWFS at the HET. The PWFS was mounted at the center of the field of the HET. We had the HET pointing fixed to a few Geo-synchronous satellites so that the test can avoid any influence from the tracker movement. We have used the Direct TV-10 (12^{th} mag) and GOES-14 satellites (11^{th} mag) as

targets for the test. We then stepped through the Spherical Aberration Corrector (SAC) in focus and tip/tilt by controlling the hexapods holding the SAC. The focus range was ±400μm and the tip/tilt range was ±40 arc-seconds. During the test, the wind speed was reaching 25mph sideways to the SAC (i.e. along the x-axis in Figure 2) therefore the tip motion (i.e. rotating the SAC about the vertical axis or φ motion in Figure 2) was greatly affected by the strong wind. However, the focus and tilt (i.e. rotating the SAC about the horizontal axis or θ motion in Figure 2) turned out to be benign to the wind. We took 5 images from the PWFS and image at each focus and tip/tilt step. Since the targets were bright enough, we limited our exposure time to less than 5 seconds to avoid pixel saturation, which is much shorter than the required exposure time for the WFS. During the test, we also turned on the DMI and TTCam so that we can correlate the PWFS estimates with those from the two devices. Since we were interested in relative motion from a certain off-set point and the DMI and TTCam are accurate to ±5μm and ±0.5 arc-seconds in peak-to-valley, respectively, a comparison between these devices and the PWFS can give us a good idea about the focus/tip/tilt estimation accuracy that we can get out of the PWFS.

Figure 17 shows the correlation between the estimate of the PWFS and those by the DMI and TTCam. Each focus/tip/tilt value of the PWFS was computed by averaging 5 frames. The RMS variation of each point is ±5.4μm in focus, ±1.6 arc-seconds in tilt or theta, and ±6.8 arc-seconds in tip or phi. These variations are apparently larger than the simulations predicted. However, the simulations did not take into account dynamic external disturbances like the strong wind we experienced during the run, which apparently affected the tilt or phi estimate from the PWFS. When correlated with the DMI and TTCam data, the focus and tip motion show remarkable consistency with the results from the two independent devices. The slope of both parameters from the PWFS remains between 0.9 and 0.95 as predicted by the lab experiment. The response from the PWFS is also remarkably linear across the range of motions, which are in fact 40 times larger in focus and 10 times larger in tip/tilt than the required ranges (Table 1).

At this time, the guide probe assembly is operational and undergoing tests and alignment procedures. One test completed so far is mapping the spherical surface for a probe and measuring run-out from that surface due to bearing imperfections. The test utilized an API Tracker3 laser tracker mounted on a mast above the guide probe assembly tracking a ½ inch ball-mounted retro reflector mounted on a guide probe arm. The guide probe is run through a raster pattern routine, with laser tracker measurements taken every 1mm of probe motion. A sphere is fit to the recorded points using New River Kinematics' Spatial Analyzer software. Deviations of the measurement data from the fit sphere can be visualized in a vector plot. The maximum deviation was measured to be 31 microns in focus[12].

2.4 Acquisition Camera (ACAM)

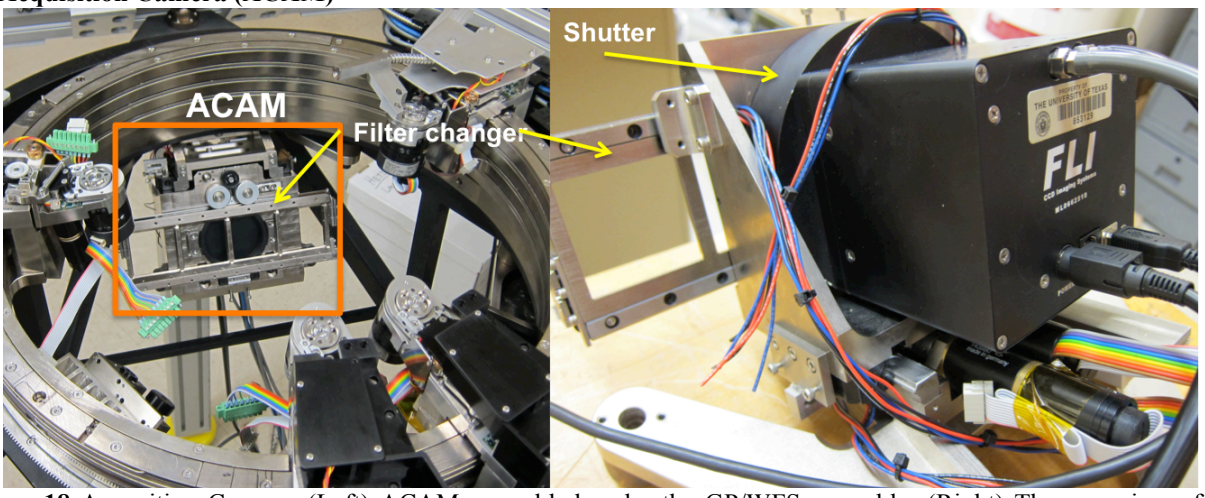

Figure 18 Acqusition Camera. (Left) ACAM assembled under the GP/WFS assembly, (Right) The rear view of the ACAM.

The ACAM (Figure 18) is located beneath the GP/WFS assembly and contains a FLI ML090000 that uses a Kodak KAF-09000 monochromatic 16-bit CCD chip with liquid-cooled TEC. The pixel format is 3056x3056 with 12μm pitch. The pixel scale is 0.068 arc-seconds and we plan to bin it by 4. It has a 3.5 arc-minutes field of view about the center of the telescope field. The camera is fed light by a pneumatically deployed fold mirror (not shown in the picture but see Ref. [12]) located opposite to the ACAM underneath the GP/WFS assembly. When the ACAM is used, the pick-off mirror extends toward the center of the beam to re-direct the central portion of the field to the ACAM. The camera is

able to focus +/-15mm from nominal along a pair of adjustable preload THK HR1530 ball guides. Actuation is by a miniature ball screw purchased from Misumi and turned by the Maxon ECmax 22 motor and gear head used in the guide probe assembly and elsewhere. A Lika linear magnetic absolute encoder with 5 microns resolution is used to measure focus position. Its SSI interface is connected directly to the Maxon EPOS2 motor controller for position control. The acquisition camera includes a four-position filter changer for 50mm square filters. The filter changer rides on a set of adjustable preload ball guides purchased from Misumi. A toothed belt is stretched along one edge of the magazine and through two idlers and a drive pulley. The drive pulley is turned by one of the same Maxon motor and gear heads. Four hall effect switches are mounted to the chassis and triggered by two magnets on the filter magazine. Each hall effect switch corresponds to a filter position and their outputs are wired to the Maxon motor controller. A homing mode is used to drive the magazine position until the desired hall effect switch is triggered. Owing to its relatively large field of view, the ACAM is to be used for acquiring and identifying a science target field, which will be used to register the other facility instruments at the central port of the focal surface, namely the High Resolution Spectrograph, Medium Resolution Spectrograph, and Low Resolution Spectrograph-2. The ACAM can also provide imaging capability for different science observations. The ACAM will also be used to occasionally monitor the plate scale variation and the image quality of the telescope.

2.5 Pupil Viewing Camera (PVCam) and Calibration Wavefront Sensor (CWFS)

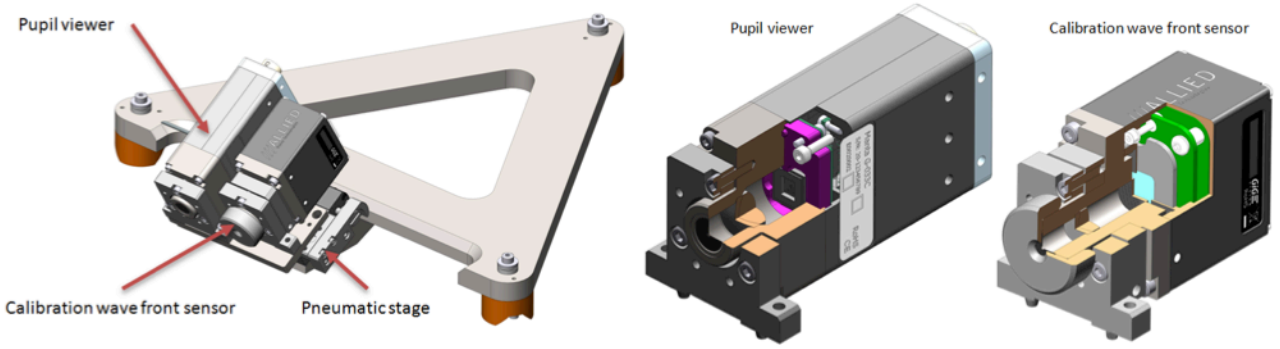

Figure 19 (Left) The PVCam and CWFS on their pneumatic stage. (Right) The section views of the solid models of the PVCam and CWFS.

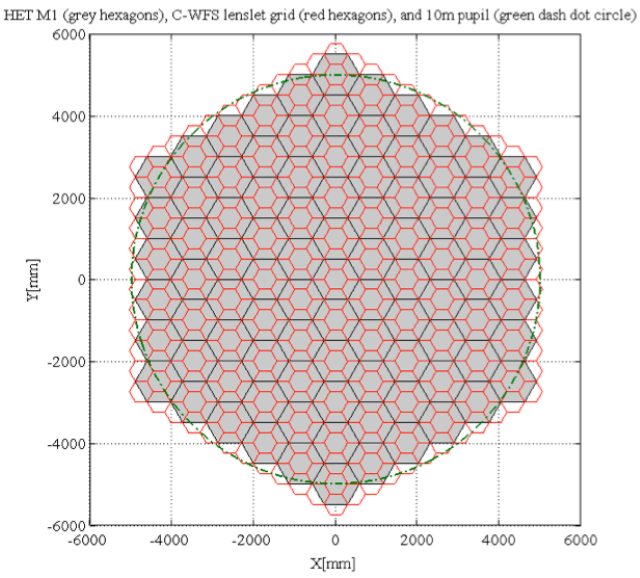

Figure 20 The sub-aperture grid of the CWFS overlaid on the HET Primary mirror segments.

The solid models of the PVCam and the CWFS are shown in Figure 19. Both optical metrology devices are located underneath the GP/WFS assembly. Both are built around AVT machine vision cameras. The pupil viewer has a collimating lens in custom housing mounted directly to a AVT Manta G-046 camera with stock C-mount bayonet removed. The CCD sensor uses a SONY ICX415 3 color 12-bit CCD chip. The pixel format is 780x580 with 8.3µm pitch. At the front of the PVCam, a field stop of 7 arc-seconds diameter is integrated in order to deal with a large pointing mismatch and at the same time to minimize stray-light into the system. The field stop is centered on the telescope field. The main function of the PVCam is to provide the image of the telescope pupil. The size of the re-imaged 10-m telescope pupil is 3.8mm in diameter on the CCD. This allows us to image individual M1 segments in three colors at a resolution of 50 pixels across mirror segment. Photometry of the segment images can give us the spectral response of the segments over time and the time-dependent mirror reflectivity degradation can be monitored in a relative sense from a particular point of time (e.g. when the

segment is re-coated). Another function of the PVCam is to monitor the moving baffle that is mounted in the exit pupil at about half way between M5 and the focal surface. The the moving baffle blocks the section of the pupil falling outside the primary mirror during a track and it is important to test if the baffle follows the primary mirror during a track. In addition, the telescope pupil measurement during different sets of tracks will verify the telescope's dynamic obscuration model that has been derived from the HET WFU Zemax design and will be used in the calibration process of the HETDEX data.

The CWFS has a custom housing for collimating optics and micro-lens array mounted to a AVT Prosilica GC2450 camera. The CCD sensor uses a Sony ICX625 monochromatic 12-bit CCD chip. The pixel format is 2448x2050 with 3.5μm pitch. The CWFS field of view is 6.4 arc-seconds in diameter and centered on the telescope field. The CWFS uses a Fused-silica hexagonal miro-lens array with 250μm pitch. Each micro-lens is f/16 and the focal length variation is at 1% level. The projected size of the 10-m telescope pupil is 5.2mm in diameter or 21 sub-apertures across the diameter. Therefore, at least 100 sub-apertures are fully illuminated in any track positions, enabling us to sense telescope aberrations higher than what the WFS in the GP/WFS assembly can provide. The aberration data from the CWFS can then be used to calibrate the signal from the WFS. As shown in Figure 20, the sub-aperture size is chosen so that there is one sub-aperture at the border of two neighboring segments. This allows us to determine the inter-segment phase errors (via Broadband phasing algorithm[11]), which is used to verify the segment piston correction from the DMI. Details of segment phasing at the HET using the CWFS is being worked out at the time of this writing.

Both the PVCam and CWFS use gigabit Ethernet communications and are air-cooled. The two devices are mounted to a Festo SLF-10 pneumatic slide to share the optical feed from a pneumatically deployed fold mirror (Figure 19, the mirror is not shown but see Ref. [12]). The pupil viewer has a tip-tilt-focus adjustable mount and the calibration wave front sensor has a tip-tilt-focus adjustment plus a rotational adjustment. A set of hall-effect switches detects position of the pneumatic stage at ends of travel.

4. METROLOGY FEEDBACK & CONTROL

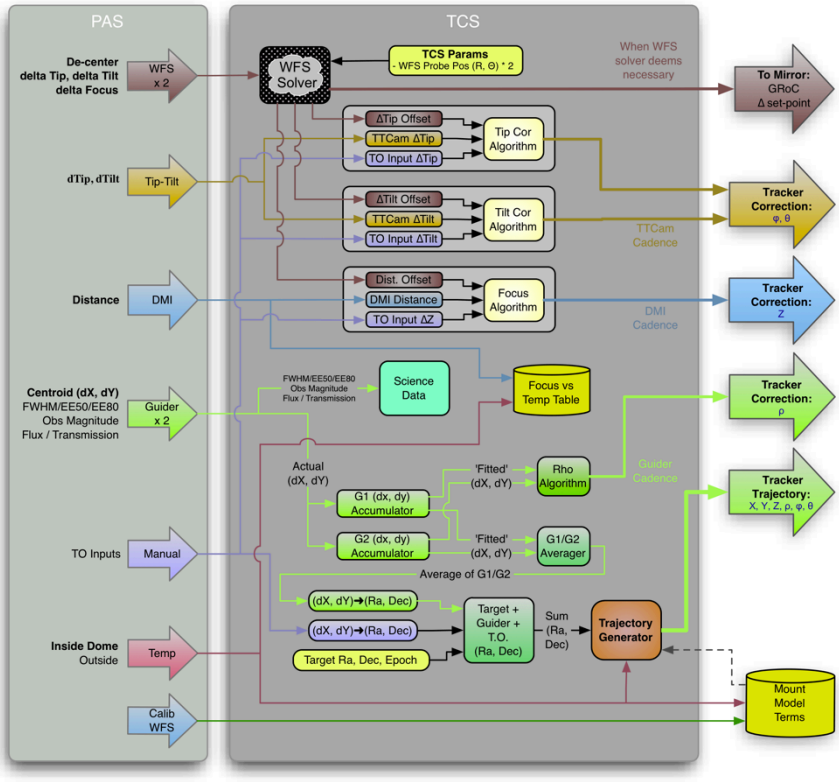

Figure 21 The metrology feedback and control flow diagram.

From the metrology systems we will have sufficiently redundant information on the WFC alignment state with respect to the primary mirror. However, there is a fundamental difference between these metrology feedbacks. TTCam and DMI will provide the mechanical alignment state of the WFC, while the GP and WFS will produce the WFC alignment control feedbacks based on optical measurements (thus yielding the optical alignment state of the WFC). Although both TTS and DMI are to be calibrated against the optical measurement by the WFS and GP so that the relation between the optical axes of TTS and DMI and those of the WFC will be known, there is a possibility that this relationship changes during the operation of the telescope due to, for example, misalignment of the internal components of the WFC (i.e. the WFC mirrors and focal plane assembly). The WFC internal components are to be rigidly mounted to their mounting

structure, but the Finite-Element Analysis of the WFC suggests that the internal mirrors and focal plane will be shifted and rotated due to variations in gravity vector and temperature during telescope operations. The internal alignment variations are expected to be repeatable so that they can be explicitly modeled or measured and then subtracted. In a situation where this is not the case due to the existence of unknown (or less accurate) telescope mount models, the WFS feedback will be used to set the fiducials of the DMI and TTS. Each metrology system will have different update rates. The TTS and DMI will have an update rate of 10 sec. The GP update rate can be made as fast as 1 ~ 5sec. The current baseline WFS update rate is 60 sec for an m_V=18 star. For brighter stars, the WFS update can be more frequent, but we plan to have the exposure longer than 15 seconds in order to sufficiently average out atmospheric aberrations which we do not wish to sense with the WFS. Given these differences between the metrology systems, it is necessary to coordinate the feedbacks from different metrology systems in order to optimally control the WFC alignment.

The chart in Figure 21 illustrates the current snapshot of the metrology feedback and control. In the control flow, there are three primary "fast" control loops running on the Payload Alignment System (PAS) computer: DMI, tip/tilt, and guide. These loops run in parallel, asynchronously, with no cross dependencies. The DMI loop reads the distance measuring interferometer to maintain the distance from the WFC/PFIP to the primary mirror. The tip/tilt loop uses the TTCam to maintain the orientation of the WFC/PFIP mechanically with respect to the primary mirror. The guide loop keeps the WFC/PFIP pointed at the target star. A slower WFS loop uses wavefront sensing to check the focus and orientation of the WFC/PFIP optically and then adjusts the offsets in the DMI and tip/tilt loops. Each time the PAS takes an image from a camera, or reads the DMI, the data are processed locally and, for example, centroids are computed. These measurements are pushed onto a queue, which is in turn read by the Telescope Control System (TCS). The raw measurements are calibrated and transformed geometrically into corrections to be applied to the tracker's trajectory. New sets of trajectory points are uploaded to the tracker on approximately 1-second intervals. As new metrology data come in on slower cadences, these points are recomputed using a simple running mean "predictive guiding" algorithm. Also, in parallel with the position and orientation data, photometric measurements from the guiders are piped to the GUI to tell the operator about current conditions, and to the science headers, to permit proper scaling of the frames making up a science dither set. As part of sensing the gross alignment of the WFC, the WFS can also sense a gross drift in the global radius of curvature (GRoC) of the primary mirror. The GRoC has essentially the same effect as the WFC defocus: blurring stellar images and adding defocus aberration to WFS signals. As a result, it is difficult to distinguish these two parameters just by analyzing the WFS aberration data and/or GP image quality data. Our plan for updating the GRoC is as follows. The DMI maintains the physical separation between the WFC and the M1 as the GRoC drifts. This will accumulate defocus aberration to the WFS signal, thereby increasing the required amount of the WFC focus correction given by the WFS. Once the amount of the *accumulated* WFS-based focus correction reaches a certain upper limit (which must be set by the required seeing-convolved image quality specification), the accumulated value is applied as change in the GRoC. At the same time, the DMI zero point is offset by this value. Although the GRoC variation leads to a change in the telescope plate scale (which can be monitored by the guider centroids and WFS tip/tilt aberrations), this variation is much less significant than the impact of GRoC on the image quality and thus may not be easily detected. However, we expect that monitoring the plate scale drift can also provide another constraint on a long-term GRoC variation.

The DMI and TTCam can also monitor the M1 segment piston/tip/tilt errors. Figure 11 shows the distance (left) and

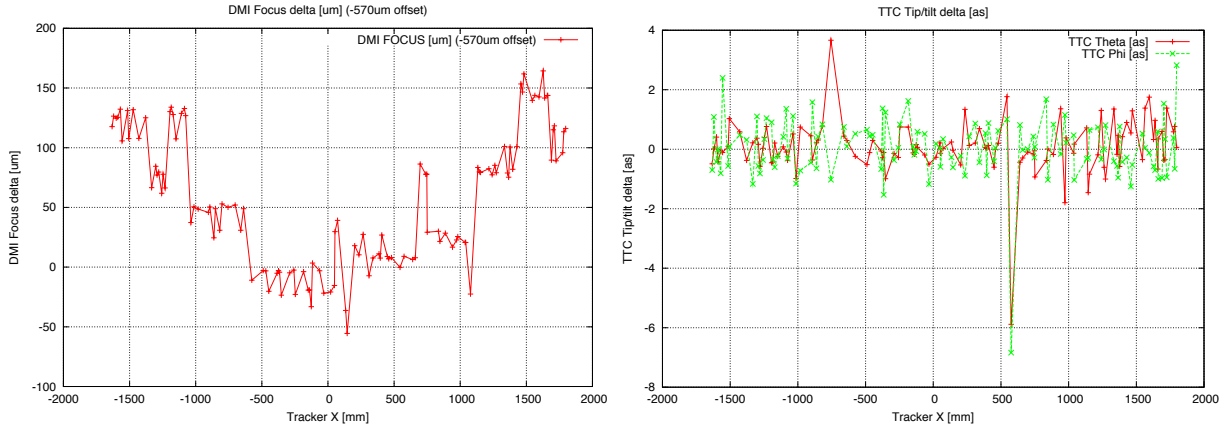

Figure 22 (Left) DMI and (Right) TTCam signal during 1hr track at the current HET.

tip/tilt measurements (right) during an hour-long track from the current DMI and TTCam in the HET. The DMI plot clearly shows a step-wise variation (amounting 50 to 70 μm) in the curve. When comparing this curve with the trajectory from the tracker, the step-wise variation appears to occur around the edges of two adjacent mirror segments. In between step-wise variations, the curve is almost flat (with ±10μm fluctuations). The points in these regions fall within a single segment. These step-like variations probably result from a combination of segment piston, tip/tilt, and figure errors. However, the TTCam measurement on the right panel shows that the WFC tip/tilt relative to the primary mirror was consistently maintained within ±2 arc-seconds along the hour-long track. A 1 arc-second segment tip/tilt leads to roughly 3μm piston at the edge of the segment. An investigation suggests that the surface figure error of the mirror segments is less than 1 wave at 632.8 nm in peak-to-peak across the M1[13], which is less than a micron in terms of surface sag value. Thus, the step-wise variation in the top plot is mostly from the segment piston error. Inversely, the plot suggests that the DMI measurement can be utilized to find appropriate segment piston corrections. In the WFU, we plan to use three DMIs for this purpose and expect that the M1 piston error can be reduced down at least to the level of the DMI accuracy observed in the left plot. Also, the TTS measurement can reveal step-wise changes between segments if there is any large segment-to-segment tip/tilt error.

5. SUMMARY

In this paper, we described the key metrology systems for active alignment of the WFC. These systems are the DMI, TTCam, GP, WFS, ACAM, PVCam, and CWFS. We plan to adopt the DMI and TTCam used in the current HET. In addition to the current DMI system, we will add two more DMI heads, three heads in total. These DMI heads will allow us to reach all mirror segments so that the segment piston errors across the M1 can be measured and corrected. During science operation, one DMI is used to maintain the mechanical separation between the WFC and the M1. The distance capture range of the DMI is 40 mm with intrinsic repeatability of 5 μm peak-to-valley. A small modification will be made to the TTCam in order to make it more compact and to operate it substantially away from the telescope optical axis. The TTCam will be used to maintain the mechanical tip/tilt of the WFC with respect to the M1. The intrinsic measurement repeatability of the TTCam is 0.5 arc-seconds in peak-to-valley. In conjunction with these two systems, we will have two guide probes and two low-order Shack-Hartmann wavefront sensors operating within the annular metrology service field at the edge of the telescope focal plane assembly. The guide probes will provide feedback on the telescope pointing, plate scale, image quality, and atmospheric transparency, while the wavefront sensors will optically monitor the gross WFC alignment with respect to the primary mirror and the variations in the telescope aberrations. The expected GP guiding accuracy is 0.25 arc-seconds or better in rms. In a rather ideal situation, the expected intrinsic WFC alignment estimation accuracy of the WFS is ±2.5μm in focus, ±0.7 arc-seconds in tip/tilt, peak-to-valley. The PWFS on-sky test at the HET indicated that the accuracy would be close to ±15μm in focus and ±4.8 arc-seconds in tip/tilt, while the accuracy can be affected by dynamic external disturbances at the telescope (e.g. strong wind). The linearity of the WFS estimation is expected to stay between 5% and 10% level over a quite large range of WFC motion (based on the PWFS on-sky tests). In the control loop, the DMI and TTCam will frequently (~ every 10 seconds) update the focus and tip/tilt feedback for the WFC alignment control, while the WFS updates the fiducial values for the DMI and TTCam every 60 seconds or 50. The combination of the WFS and DMI feedback will be used to monitor and control the global radius of curvature of the M1 during operation. There will also be a higher-order Shack-Hartmann wavefront sensor. The CWFS will have denser sub-apertures than the WFS will have. This will enable finer sampling of the telescope wavefront error and thus can provide reference signals against which the WFS are calibrated. The CWFS will be also used during the on-sky installation and commissioning of the WFU to assist the mount modeling and various calibration activities. This will be the truth sensor for calibrating the DMI and TTCam as well. This sensor will also be used to establish and verify various telescope mount model terms during WFU installation and commissioning. Together, these systems can provide fully redundant alignment and pointing information for the telescope, keeping the WFC in focus and suppressing alignment-driven field aberrations. In addition, there will be a pupil-viewing camera (PVCam) \. The PVCam will enable us to monitor the reflectance of the segment mirror coating and the moving baffle position relative to the primary mirror.

ACKNOWLEDGEMENTS

HETDEX is run by the University of Texas at Austin McDonald Observatory and Department of Astronomy with participation from the Ludwig-Maximilians-Universität München, Max-Planck-Institut für Extraterrestriche-Physik (MPE), Leibniz-Institut für Astrophysik Potsdam (AIP), Texas A&M University, Pennsylvania State University, Institut für Astrophysik Göttingen, University of Oxford and Max-Planck-Institut für Astrophysik (MPA). In addition to

Institutional support, HETDEX is funded by the National Science Foundation (grant AST-0926815), the State of Texas, the US Air Force (AFRL FA9451-04-2-0355), and generous support from private individuals and foundations.

REFERENCES

[1] G.J. Hill, J.A. Booth, M.E. Cornell, J.M. Good, K. Gebhardt, H.J. Kriel, H. Lee, R. Leck, P.J. MacQueen, D.M. Perry, M.D. Rafal, T.H. Rafferty, C. Ramiller, R.D. Savage, C.A. Taylor III, B.L. Vattiat, L.W. Ramsey, J.H. Beno, T.A. Beets, J.D. Esguerra, M. Haueser, R.J. Hayes, J.T. Heisler, I.M. Soukup, J.J. Zierer, Jr., M.S. Worthington, N.T. Mollison, D.R. Wardell, G.A. Wedeking, "Current status of the Hobby-Eberly Telescope wide field upgrade," Proc. SPIE, **8444**-19 (2012).

[2] G. J. Hill, et al., "The Hobby-Eberly Telescope Dark Energy Experiment," AIP Conference Proceedings, 773 224-223 (2004).

[3] J. H. Burge, S. D. Benjamin, M. B. Dubin, S. M. Manuel, M. J. Novak, Chang Jin Oh, M. J. Valente, C. Zhao, J. A. Booth, J. M. Good, G. J. Hill, H. Lee, P. J. MacQueen, M. D. Rafal, R. D. Savage, M. P. Smith, B. L. Vattiat, "Development of a wide-field spherical aberration corrector for the Hobby Eberly Telescope", Proc. SPIE, **7733**-51 (2010).

[4] H. Lee, et al., "Metrology systems for the active alignment control of the Hobby-Eberly Telescope wide-field upgrade," Proc. SPIE, 7739-28 (2010).

[5] P. Palunas, et al., "Imaging performance of the Hobby-Eberly Telescope," Proc. SPIE **6267**-127 (2006).

[6] M. T. Adams, et al., "Hobby-Eberly Telescope Segment Alignment Maintenance System," Proc. SPIE **4837,** 693-701 (2003).

[7] M.J. Wolf, M. Ward, J.A. Booth, A. Wirth, G.L. Wesley, D. O'Donoghue, & L. Ramsey, "Mirror Alignment Recovery System on the Hobby-Eberly Telescope", in Large Ground-Based Telescopes, Proc SPIE 4837, 714, 2003.

[8] Fogale Nanotech, "Low coherence interferometric sensor, Model: LISE-LS 40, HET 2Channel," User's Manual (2005).

[9] J.D. Murphy, G.J. Hill, P.J. MacQueen, T. Taylor, I. Soukup, W. Moreira, M.E. Cornell, J. Good, S. Anderson, L. Fuller, H. Lee, A. Kelz, M. Rafal, T. Rafferty, S. Tuttle, & B. Vattiat, "The Effects of Motion and Stress on Optical Fibers", Proc. SPIE, 8446-207 (2012).

[10] H. Lee, Gary J. Hill, Michael Hart, and Marc D. Rafal, "Analysis of active alignment control of the Hobby-Eberly Telescope Wide Field Corrector using Shack-Hartmann wavefront sensors," Proc. SPIE, **7738**-18 (2010).

[11] Gary Chanan, Mitchell Troy, Frank Dekens, Scott Michaels, Jerry Nelson, Terry Mast, and David Kirkman, "Phasing the Mirror Segments of the Keck Telescopes: The Broadband Phasing Algorithm," Applied Optics, **37**, 140-155 (1998).

[12] B.L. Vattiat, G.J. Hill, H. Lee, D.M. Perry, M.D. Rafal, T. Rafferty, R. Savage, C.A. Taylor III, W. Moreira, M.P. Smith, "Design, testing, and performance of the Hobby Eberly Telescope prime focus instrument package," Proc. SPIE, 8446-269 (2012).

[13] H. Lee, Gary J. Hill, and Michael Hart, "Phase retrieval analysis of the Hobby-Eberly Telescope primary mirror segment surface error and its implications for the wavefront sensing in the new wide-field upgrade," Proc. SPIE, **7738**-58 (2010).